*Original Article*

DOI: 10.5582/irdr.2023.01108

# Role of IFITM2 in osteogenic differentiation of C3H10T1/2 mesenchymal stem cells

**Yongtao Zhang[1], Xiangdong Li[2], Shanshan Zhang[1], Junfeng Li[1], Meilin Liu[1], Yanqin Lu[1,3,*], Jinxiang Han[1,3,*]**

[1] Key Laboratory for Biotech Drugs of the National Health Commission, Key Laboratory for Rare & Uncommon Diseases of Shandong Province, Biomedical Sciences College & Shandong Medicinal Biotechnology Centre, Shandong First Medical University & Shandong Academy of Medical Sciences, Ji'nan, Shandong, China;
[2] Department of Clinical Laboratory, The First Affiliated Hospital of Shandong First Medical University & Shandong Provincial Qianfoshan Hospital, Ji'nan, Shandong, China;
[3] Department of Endocrinology and Metabology, The First Affiliated Hospital of Shandong First Medical University & Shandong Provincial Qianfoshan Hospital, Ji'nan, Shandong, China.

**SUMMARY** Interferon-inducible transmembrane (IFITM) are a family of small proteins localized to plasma and endolysosomal membranes. Their functions beyond restricting viral entry and replication have been revealed in recent years. IFITM5 is involved in bone mineralization and is an osteogenic cell surface marker. IFITM1 and 3 interact with desmin and myosin, and are involved in myogenic differentiation. This study found upregulation of *Ifitm2* during osteogenic differentiation of C3H10T1/2 cells. This positively correlated to the expression of osteogenic differentiation markers *Col1a1, Alp, Runx2*, and *Ocn*. Knockdown of *Ifitm2* by siRNAs inhibited osteogenic differentiation, calcium deposition, and osteogenic marker expression of C3H10T1/2 cells. The osteoblast transcriptome revealed that knocking down *Ifitm2* affected the expression Wnt signaling pathway-related genes, including Wnt family members, their receptors Lrp, Frizzled, and Lgr, and transmembrane molecule Rnf43 that suppresses the Wnt signaling pathway. Luciferase assays indicated enhancement of canonical Wnt signaling pathways by *Ifitm2* overexpression. Furthermore, IFITM2 was colocalized in the metaphyseal bone and growth plate of the mouse tibial bone with SP7, a transcription factor essential for osteoblast differentiation and bone formation. These findings reveal a possible novel function and potential mechanisms of *Ifitm2* in osteogenic differentiation.

***Keywords*** IFITM2, osteogenic differentiation, Wnt/β-catenin signaling pathway, TOP/FOP assay, C3H10T1/2 cells

## 1. Introduction

Mesenchymal stem cells can differentiate into mature osteoblasts lining the bone surface and osteocytes embedded in bone (*1*). Osteogenesis is a three-step process consisting of the proliferative phase, matrix maturation, and mineralization (*2*). The process is characterized by distinctive sequentially expressed osteoblast markers, including alkaline phosphatase (ALP), type I collagen (Col1), osteopontin (OPN), bone sialoprotein (BSP), and osteocalcin (OCN) (*3-7*). The effects of interferon (IFN) on differentiation of osteoblastic cells have recently drawn attention (*8,9*). Even without exogenous IFN and virus infection, in a cell model of osteogenic differentiation, the cells spontaneously produce endogenous IFN that increases expression of interferon-stimulated genes, including interferon-inducible transmembrane (IFITM) proteins (*10*).

IFITM proteins belong to the small interferon-stimulated family with molecular masses ranging from 10 to 20 kDa (*11*). The family members include IFITM1, IFITM2, IFITM3, IFITM5, and IFITM10 in humans, and IFITM1, IFITM2, IFITM3, IFITM5, IFITM6, IFITM7 and IFITM10 in mice (*12,13*). Except for IFITM3, IFITMs are highly expressed in rat bone marrow (*14*). IFITM1–3 play a vital role in blocking viral infection (*15,16*). IFITMs are increasingly thought to have a role in cancer and innate immunity (*17*). We previously found upregulation of IFITM1–3 during myogenic differentiation, and IFITM1 and 3 interact with desmin and myosin (*18*). Hence, the functions of IFITMs

extend to multiple lineages of differentiation. The study investigated *Ifitm2* expression during osteogenic differentiation and the related signaling pathways.

## 2. Materials and Methods

### 2.1. Cell culture and osteogenic differentiation of C3H10T1/2 cells

C3H10T1/2 cells were cultured in high-glucose Dulbecco's modified Eagle's medium supplemented with 10% (v/v) fetal bovine serum, 2 mM glutamine, 100 U/mL penicillin, and 100 μg/mL streptomycin at 37°C with 5% $CO_2$. Osteogenic differentiation of C3H10T1/2 cells was performed in 6- or 24-well plates. At 24 h post-seeding, cells were cultured in osteogenic differentiation medium containing 10 mM β-glycerophosphate, 100 nM dexamethasone, and 0.2 mM ascorbic acid. C3H10T1/2 cells were osteogenically stimulated for 14 days with medium exchanges every 3 days. The osteogenic differentiation capacity was determined by alizarin red S staining.

### 2.2. Alizarin red S staining

C3H10T1/2 cells were washed with PBS and fixed with 4% paraformaldehyde at room temperature for 15 min. After rinsing with PBS twice, the cells were stained with a 0.2% alizarin red S solution at room temperature for 20 min and then washed with deionized water until the supernatant was colorless. Stained C3H10T1/2 cells were imaged using a digital camera (Canon, Japan). After imaging, 10% cetylpyridinium chloride (Sangon Biotech, China) was applied in the dark for 30 min, and then 100 μL was transferred to a 96-well plate to measure the OD value at 560 nm. Analyses were performed in at least three independent experiments. Absorbance at day 0 was used to normalize the alizarin red S staining results.

### 2.3. RNA extraction and RT-qPCR

Total RNA was isolated from C3H10T1/2 cells cultured in differentiation or normal media using a FastGene RNA Basic Kit (Takara, Japan) in accordance with the manufacturer's instructions. RNA purity and integrity were evaluated using a NanoDrop 2000 spectrophotometer. After digestion with DNase I (Takara, Japan), 1 μg total RNA was reverse transcribed to cDNA using a ReverTra Ace qPCR RT Kit (Takara, Japan). Quantitative PCR was performed using 2× SYBR Green qPCR Mix (SparkJade, Bio, China) and a LightCycler 480. PCR conditions were as follows: initial 5 min denaturation at 95 ℃, followed by 45 cycles of amplification at 95 ℃ for 10 sec, 60 ℃ for 10 sec and 72 ℃ for 15 sec. To quantify the expression of each gene of interest, mRNA expression levels were normalized to the mRNA level of glyceraldehyde 3-phosphate dehydrogenase (GAPDH). Relative gene expression was calculated with the $2^{-\Delta\Delta Ct}$ method. Each sample was analyzed in triplicate. Primer sequences were as follows: *Gapdh*: 5′-CATCCCAGAGCTGAACG-3′ (forward), 5′-CTGGTCCTCAGTGTAGCC-3′ (reverse); *Col1a1*: 5′-GCTCCTCTTAGGGGCCACT-3′ (forward), 5′-ATTGGGGACCCTTAGGCCAT-3′ (reverse); *Alp*: 5′- GCCCGGCCGAGTACA-3′ (forward), 5′-CTGGCCAGAAACTTCACCTT-3′ (reverse); *Runx2*: 5′-ACAGAGCTATTAAAGTGACAGTGGAC-3′ (forward), 5′- GGCGATCAGAGAACAAACTAGG 3′ (reverse); *Ocn*: 5′-GCGCTCTGTCTCTCTGACCT-3′ (forward), 5′-TTCAGGAGGGTAGTTACCCAAA-3′ (reverse).

### 2.4. Western blotting

C3H10T1/2 cells in a 6-well plate were washed with cold PBS. Then, the cells were lysed in 200 μL RIPA lysis buffer with 1% PMSF (Cwbio, China) at 4°C. The extracted proteins were quantified using a BCA protein concentration assay kit (Biosharp, China). Protein samples (20 μg/lane) were resolved by 12% SDS-PAGE. Proteins were then transferred to a polyvinylidene fluoride membrane (0.45 μm, Biosharp). The membrane was blocked with 5% dry skim milk in Tris-buffered saline containing 0.1% Tween 20 (TBST) for 2 h at room temperature.

The membrane was incubated with a primary antibody against COL1A1 (1:2000, 67288-1-Ig, Proteintech, USA), ALP (1:2500, PA5-63148, Thermo Fisher, USA), RUNX2 (1:1000, 82636-2-RR, Proteintech), OCN (1:500, 3418-1-AP, Proteintech), IFITM2 (1:1000, bs-15517R, Bioss, China), or GAPDH (1:3000, ab8245, Abcam, USA) overnight at 4°C. After washing with 0.1% Tween in PBS, the membrane was incubated with an anti-rabbit-horseradish peroxidase-conjugated secondary antibody (1:2000, SA00001, Proteintech) for 1 h at 37°C. A Super-sensitive ECL chemiluminescent substrate kit (Biosharp, China) was used to develop protein bands. ImageJ-win64 (Rawak Software Inc., Stuttgart, Germany) was used for densitometry.

### 2.5. siRNA transfection

Small interfering RNA based on our previous study (*18*) and directed against mouse *Ifitm2* was synthesized by GenePharma (Shanghai, China). Before siRNA transfection, C3H10T1/2 cells were seeded at $2 \times 10^5$ cells/well in 6-well plates in serum and antibiotic-free DMEM. Transfections were performed with siRNA-*Ifitm2* or negative control siRNA (si-NC) using ExFect transfection regent (Vazyme, China) in accordance with the manufacturer's instructions. After 6 h of transfection, the medium was replaced with osteogenic differentiation medium. After 5 days, proteins were extracted for

western blotting, and total RNA was extracted for RNA-sequencing analysis.

2.6. RNA-seq and bioinformatics analysis

Total RNA was extracted using an RNeasy Mini Kit (QIAGEN, China), following the manufacturer's instructions. Two micrograms of RNA were used as the input material for the RNA sample preparation. Sequencing libraries were generated using a NEBNext Ultra RNA Library Prep Kit for Illumina (#E7530L, NEB, USA), following the manufacturer's recommendations. Index codes were added to attribute sequences to each sample. The libraries were sequenced using a NovaSeq 6000 (pair-end 150 bp). All reads were mapped to the mouse reference genome using HISAT2 (v.2.2.1) as reported previously (*19*). RNA counts were generated by *featureCounts* (v.2.0.0) (*20*). Differential expression analysis was implemented using the edgeR package (v.3.34.1) as reported previously (*21*). Genes with an expression fold change of $\geq 1.5$ or $\leq 1.5$ and adjusted P-value of $< 0.05$ were identified as significantly differentially expressed genes. For further analysis, a volcano plot was generated by the ggplot2 R package. Heat maps were generated by the pheatmap R package.

Cluster and pathway analyses were performed using the KEGG pathway database (*http://www.kegg.jp/kegg/*) and DAVID bioinformatics resources 6.8 (*https://david.ncifcrf.gov/*). Enriched pathways were ranked using the combined score calculated by the software. To perform gene ontology (GO) analysis, data of the function annotation diagram were obtained using the DAVID website, and data with $P < 0.05$ were selected. Data processing and mapping were performed using R-project (v4.0.5) and Rstudio software (v1.3.1093).

2.7. TOP/FOP flash luciferase reporter assay

HEK293T cells were seeded into a 96-well plate at $1 \times 10^4$ cells per well. Then, 250 ng TOP/FOP, 50 ng pTK-RL plasmid, and 100 ng pMCV6-Ifitm2 overexpression vector or control were transiently cotransfected into the cells using ExFect Transfection Reagent (Vazyme). The activities of firefly and Renilla luciferase reporters were measured in triplicate at 48 h post-transfection using the Duo-Lite Luciferase Assay System (Vazyme) in accordance with the manufacturer's instructions. Firefly luciferase activity was normalized to the Renilla luciferase activity. The TOP/FOP ratio was used to indicate β-catenin-driven transcription.

2.8. Immunofluorescence staining

C3H10T1/2 cells were fixed with 4% paraformaldehyde in phosphate-buffered saline, permeabilized with 0.25% Triton X-100, and blocked in a blocking solution (2% glycine, 2% bovine serum albumin, 5% fetal bovine serum, and 50 mM $NH_4Cl$ in phosphate-buffered saline) for 1 h. Then, the cells were incubated with primary antibodies for 12 h at 4℃ and then with corresponding secondary antibodies conjugated to various fluorescent dyes. For nuclear staining, the cells were incubated with 1 μg/mL DAPI (Sigma, USA) for 10 min at room temperature. After washing with PBS, the cells were subjected to microscopy.

2.9. Double immunofluorescence staining of paraffin-embedded sections

The animal study was approved by ethics committee of Shandong First Medical University & Shandong Academy of Medical Sciences, and was performed in accordance with ethical standards stated in the 1964 Declaration of Helsinki and its later amendments. The tibia was harvested from 15-week-old male mice. Specimens were immersed in paraffin and then sectioned. Double immunofluorescence staining was performed on 5-μm-thick paraffin-embedded sections of formalin-fixed mouse tibial samples. Samples were deparaffinized and rehydrated. After blocking with normal goat serum for 30 min at room temperature, a rabbit anti-IFITM2 antibody (1:500, bs-15517R, Bioss) was applied at 4°C overnight, followed by an Alexa 488-conjugated goat anti-rabbit IgG secondary antibody (1:500, A-11001, Thermo Fisher) for 1 h at room temperature. Additional immunofluorescence staining was then performed by incubation with an anti-SP7 primary antibody (1:500, Ag29889, Proteintech), for 1 h at room temperature, followed by incubation with an Alexa Fluor 594-conjugated fluorescent goat anti-mouse IgG secondary antibody (1:100, A-11005, Thermo Fisher) for 1 h at room temperature. After washing with PBS, 10 μg/mL DAPI was applied in the dark for 10 min. Samples were sealed with an anti-fluorescence attenuation sealing sheet. Images were obtained under a fluorescence microscope.

2.10. Statistical analysis

Results are presented as the mean ± standard error of the mean. To identify significant differences, statistical comparisons were made by one-way ANOVA and the Tukey multiple comparisons test using GraphPad Prism software (v.8.0) (GraphPad Software Inc, USA). $P < 0.05$ was considered statistically significant. All experiments were repeated at least three times.

**3. Results**

3.1. *Ifitm2* is upregulated during osteogenic differentiation of C3H10T1/2 cells

Calcium deposition of C3H10T1/2 cells during osteogenic differentiation was detected by alizarin red S staining. After 5, 7, 10, and 14 days, the area of red

staining in the surrounding material was increased gradually, indicating enhanced precipitation of calcium salts as induction time increased (Figure 1A). Quantitative analysis of osteogenic mineral deposition indicated a significant difference between the osteogenic differentiation group at day 5 and later days compared with day 0, which was uninduced (Figure 1B). Analysis of osteogenic differentiation markers was performed at 0–14 days of incubation in osteogenic differentiation medium. mRNA and protein expression levels of *Col1a1*, *Alp*, *Runx2*, and *Ocn* at days 10 and 14 after osteogenic differentiation induction was consistent and significantly increased ($P < 0.01$) (Figure 1C, D).

RT-qPCR analysis indicated that C3H10T1/2 cells in osteogenic induction medium at day 7 showed the highest expression of *Ifitm2*, but no significant increase was found at days 3 and 5 (Figure 2A). Overall trends showed an increase in IFITM2 protein expression during osteogenic differentiation of C3H10T1/2 cells with higher expression on days 3 and 5 compared with day 0 before induction and slightly decreased expression at day 7 ($P < 0.01$) (Figure 2B). Immunofluorescence also showed an increase in IFITM2 expression after 5 days of osteogenic induction compared with day 0 ($P < 0.01$) (Figure 2C).

### 3.2. siRNA downregulates *Ifitm2* expression during osteogenic differentiation of C3H10T1/2 cells

We hypothesized that *Ifitm2* plays a role in calcium homeostasis during osteogenic differentiation of C3H10T1/2 cells. Therefore, we silenced *Ifitm2* gene expression to examine its effect on mineralization of C3H10T1/2 cells during osteogenic differentiation (Supplement Figure S1, *http://www.irdrjournal.com/action/getSupplementalData.php?ID=176*). Alizarin red S staining showed reduced calcium deposition of osteogenically induced cells transfected with specific *Ifitm2* siRNAs ($P < 0.01$) (Figure 3A). Quantitative analysis showed that C3H10T1/2 cells with *Ifitm2* knockdown exhibited low calcium deposition at day 5 after osteogenic induction, whereas calcification was observed in si-NC and mock groups (Figure 3B). Regarding osteogenic marker genes, the expression levels of COL1A1, ALP, RUNX2, and OCN were significantly low in *Ifitm2* knockdown groups, which further indicated the involvement of *Ifitm2* in osteoblastic differentiation ($P < 0.01$) (Figure 3C, D).

### 3.3. RNA-seq and bioinformatics analysis

We used RNA-seq and bioinformatics analysis to assess gene expression changes triggered by *si-Ifitm2* transfection. A volcano plot of RNA-seq data revealed that 2,064 genes were upregulated (red) and 1,848 were downregulated (blue) after *Ifitm2* knockdown [fold change ≥ 1.5, false discovery rate (FDR) < 0.01] (Figure 4A). Heat map analysis revealed distinct genes after *Ifitm2* knockdown (Figure 4B, C; details on the genes are displayed in Supplementary Table S1, *http://www.irdrjournal.com/*

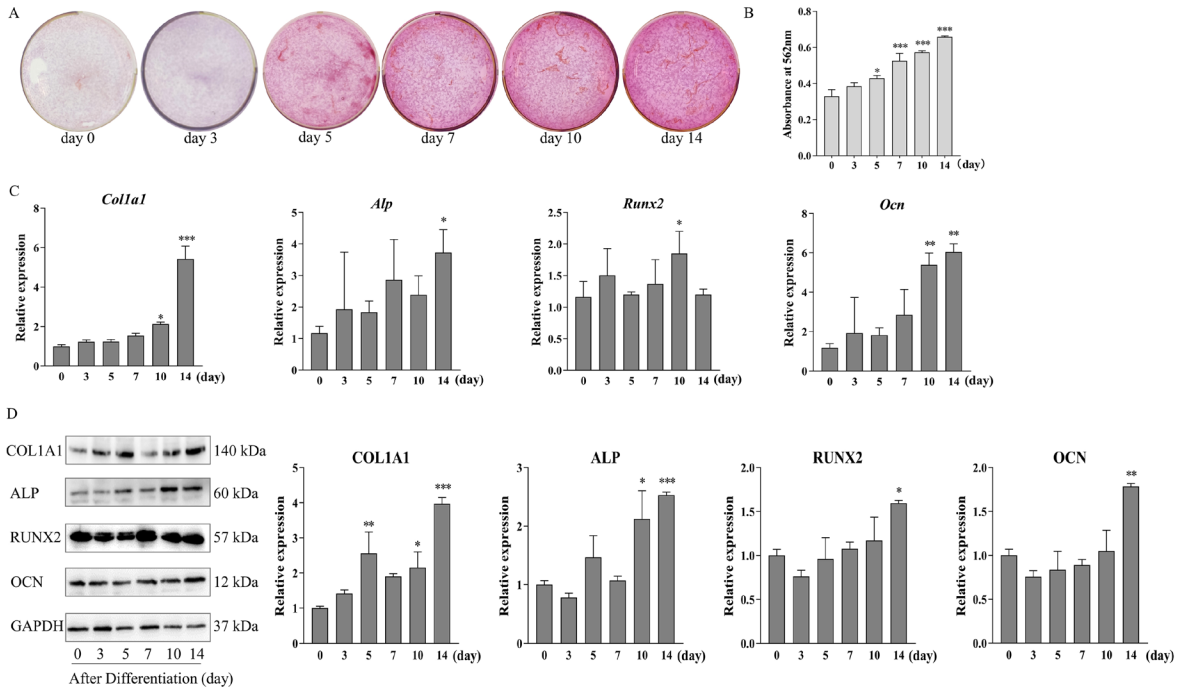


**Figure 1. Alizarin red S staining and osteogenic biomarker expression of C3H10T1/2 cells at various days of osteogenic induction. (A)** Representative alizarin red S staining of cells in 24-well plates. **(B)** Quantification of alizarin red S staining showed an increase in calcium deposition after osteogenic induction (**$P < 0.01$ *vs.* day 0 group). **(C)** Expression levels of *Col1a1*, *Alp*, *Runx2*, and *Ocn* measured by RT-qPCR. **(D)** Representative bands of COL1A1, ALP, RUNX2, OCN, and GAPDH in western blots. Semi-quantification of the band intensity in western blots is shown. Protein levels were normalized to GAPDH. *$P < 0.05$, **$P < 0.01$, and ***$P < 0.001$ *vs.* day 0 group.

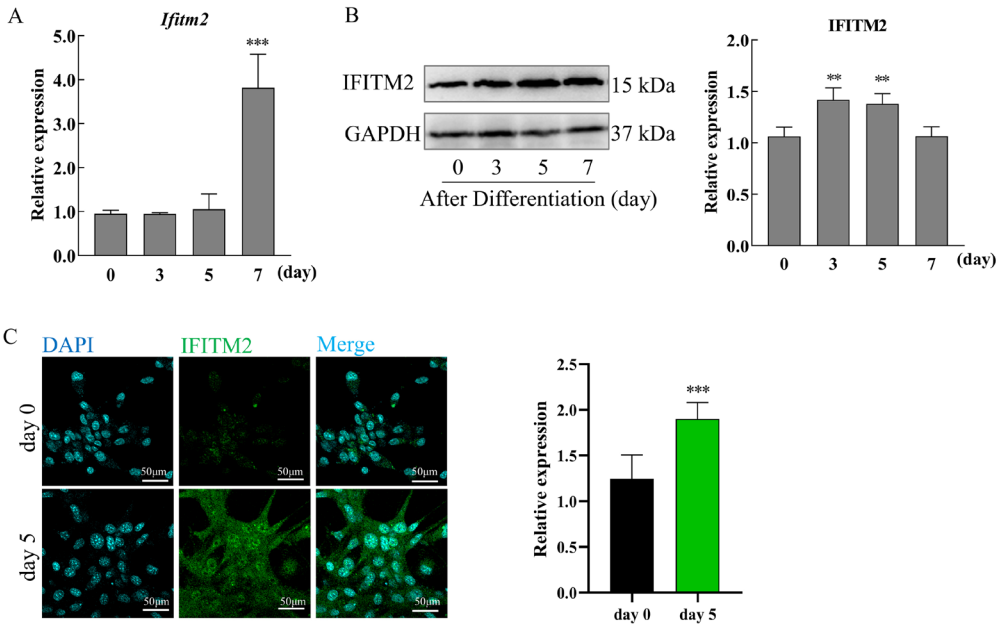


**Figure 2. Increased expression of IFITM2 during osteoblastic differentiation of C3H10T1/2 cells. (A)** Relative expression of *Ifitm2* mRNA measured by RT-qPCR after osteogenic induction for 3, 5, and 7 days. **(B)** Representative bands of IFITM2 in western blots and densitometry after osteogenic induction for 3, 5, and 7 days. Protein levels were normalized to GAPDH. **(C)** Immunofluorescence staining of IFITM2 (green) in C3H10T1/2 cells without or with osteogenic induction (day 5). Scale bars, 50 μm. Nuclei were visualized by DAPI staining. Quantitative analysis of the relative fluorescence intensity by one-way ANOVA is shown ($n = 3$). $^{**}P < 0.01$, and $^{***}P < 0.001$.

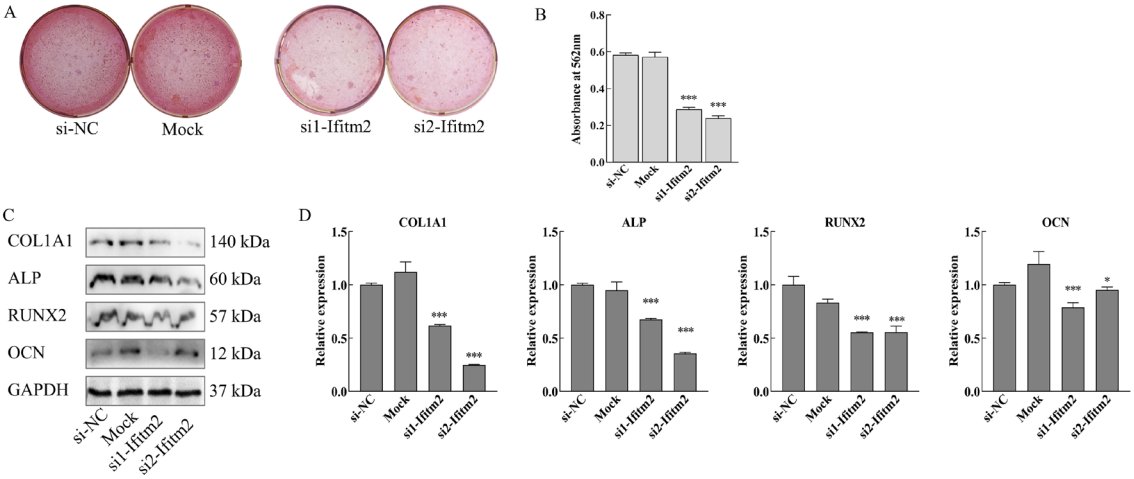


**Figure 3. Alizarin red S staining and osteogenic biomarker expression of C3H10T1/2 cells transfected with si-*Ifitm2* after 5 days of osteogenic induction. (A)** Alizarin red S staining indicated a decrease in calcium deposition in the si- *Ifitm2* group compared with siRNA negative control (si-NC) and transection reagent only (mock) groups. **(B)** Quantification of alizarin red S staining indicated that si-*Ifitm2* reduced the mineralization capacity from 49.19% to 41.89% compared with si-NC. **(C)** Representative bands of COL1A1, ALP, RUNX2, OCN, and GAPDH in western blots. **(D)** Quantification of the band intensities. Protein levels were normalized to GAPDH. Magnification: ×10. $^{*}P < 0.05$, $^{***}P < 0.001$.

*action/getSupplementalData.php?ID=177*). Clearly, *Ifitm2* knockdown by siRNAs changed the expression of genes involved in the Wnt signaling pathway, including Wnt receptors *Lgr4*, *Fzd1*, *Fzd3-7*, *Lrp8*, and *Lrp11*, *Wnt* family members *Wnt4*, *Wnt6*, *Wnt10a*, and *Wnt10b*, and *Znrf1* and *Rnf43* (Figure 4C).

GO analysis was performed to evaluate related biological processe (BP), cell components (CC) and molecular functions (MF) of the identified genes on the basis of their variability ranking. GO enrichment analyses revealed 1174 BP entries involving the ncRNA metabolic process, ncRNA processing, ribonucleoprotein complex biogenesis, muscle tissue development, tRNA metabolic process, ribosome biogenesis, negative regulation of cell cycle, 150 CC entries involving the transcription regulator complex, nuclear speck, preribosome, spindle, spliceosomal complex, nuclear envelope, and 149 MF entries involving the inositol phosphate phosphatase activity, histone deacetylase binding, protein kinase regulator activity, RNA methyltransferase activity,

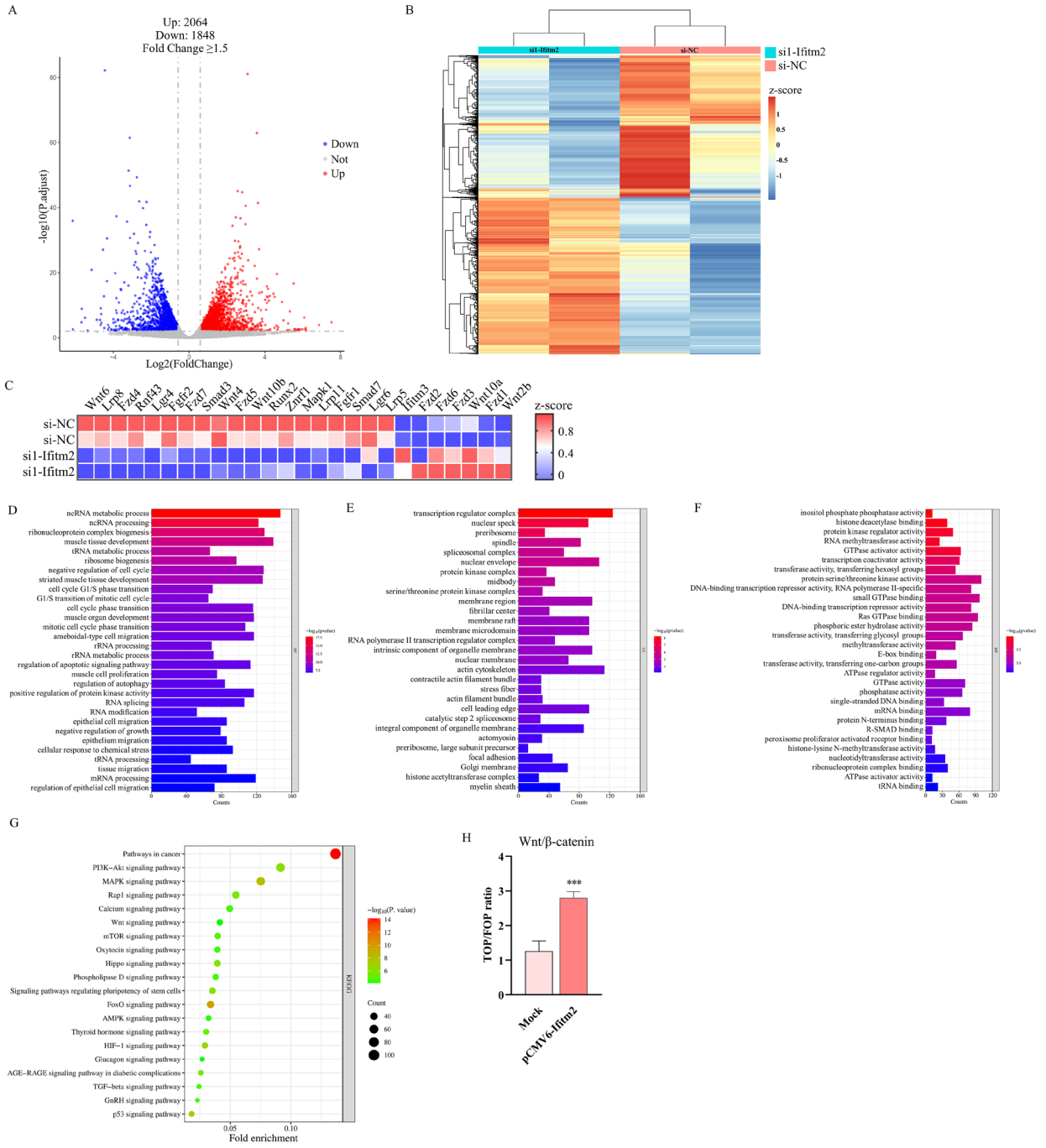


**Figure 4. Volcano plot, heat map, GO, and KEGG analyses of RNA-sequencing data.** **(A)** Volcano plots of significantly differentially expressed genes (FDR < 0.05 and |FC| ≥ 1.5; red, upregulated; blue, downregulated). **(B)** Heat map showing 3912 significantly (FDR < 0.05) differentially expressed genes between si1-*Ifitm2* and si-NC groups. Each row of the heat map represents the z-score transformed $\log_2$(1+FPKM) values of one differentially expressed gene across all samples (blue, low expression; red, high expression). **(C)** Significantly differentially expressed genes related to the Wnt signaling pathway. **(D–F)** Biological process (top 30), cellular components (top 30), molecular functions (top 30), and **(G)** KEGG enrichment analysis (top 20) of differentially expressed genes, respectively. **(H)** TOP/FOP luciferase reporter assays in HEK293T cells. TOP/FOP luciferase reporter activity was enhanced by *Ifitm2* overexpression.

GTPase activator activity, transcription coactivator activity (Figure 4D-F).

KEGG pathway analysis showed that the genes were mainly enriched in pathways in cancer, the PI3K-Akt signaling pathway, MAPK signaling pathway, Wnt signaling pathway, and signaling pathways regulating pluripotency of stem cells (Figure 4G). Among the dysregulated genes, we focused on the Wnt/β-catenin pathway and confirmed the results using a dual luciferase reporter assay. TOP/FOP luciferase reporter assays indicated that *Ifitm2* overexpression promoted luciferase activity to 2.2 fold (Figure 4H).

### 3.4. IFITM2 expression in mouse tibial tissue

To investigate the distribution of IFITM2 in bone-forming

tissue, we performed double immunofluorescence staining of mouse hind limb tissue sections to observe cells undergoing osteogenic differentiation. DAPI stains nuclei specifically (Figure 5A, E and I), IFITM2 were mainly detected in in growth plate cartilage and the trabecular bone area on the growth plate that has a high bone remodeling activity (Figure 5B, F and J). SP7 is a key transcriptional determinant of bone-secreting osteoblasts. It was expressed also in osteoblast on the surface of trabecular bone and cartilage (Figure 5C, E and K). Co-staining revealed that the entire tibia bone was positive for IFITM2 and SP7, which co-localized in the articular cartilage and metaphyseal bone (Figure 5D, H and L).

## 4. Discussion

Mesenchymal cells are ideal for stem cell-based therapy and have the capacity to differentiate into osteoblasts, chondrocytes, adipocytes, and myoblasts (*1,22*). Osteoblastogenesis is tightly regulated by complex cytokine networks under physiological and pathophysiological conditions (*2*). The IFITM family is well known for their functions in viral infection and innate immunity (*17,23-25*). IFITM5 is an osteoblast-specific membrane protein and functions as a positive regulatory factor for bone mineralization (*26,27*). IFITM5 affects Wnt signaling during tooth root development, although their interactions remain unclear (*28*). Wnt/β-catenin signaling is a major signaling pathway regulating skeletal mineralization (*29*). Downregulation of Wnt/β-catenin signaling by knockout of β-catenin in odontoblasts and cementoblasts inhibits tooth root development *in vivo* and *in vitro* (*30*). In our study, the expression of Wnt family members and their receptors, including *Lrp*, *fizzled*, and *Lgr*, was changed by downregulating *Ifitm2* expression. Moreover, expression of Rnf43, a transmembrane molecule that downregulates Wnt signaling, was decreased (*31*).

In the IFITM family, IFITM2 is a relatively newly evolved gene, and it is only present in *Homo sapiens*, *Gorilla gorilla*, and *Pan paniscus* of 26 primate species (*32*). Structurally, unlike IFITM1, which has an extended C-terminal, IFITM2 and IFITM3 have extended N-termini with an extra 20 or 21 amino acids (*33*). IFITM2 restricts entry of the CXCR4-tropic virus (*17*) and is positively associated with malignant gliomas. Enhanced *IFITM2* expression in glioblastomas predicts a malignant phenotype (*34*). In colon cancer, *IFITM2* is a novel p53-independent proapoptotic gene and highly expressed (*35*). Therefore, it is a potential therapeutic target for gastric and other cancers (*36*).

In this study, we found that *Ifitm2* was involved in osteogenic differentiation of C3H10T1/2 cells. It was upregulated during osteogenic differentiation, and knocking down *Ifitm2* led to downregulation of osteogenesis markers. Transcriptome profiling and TOP/FOP assays revealed the involvement of Wnt/β-catenin signaling induction in *Ifitm2* overexpression, which indicated a potential interaction of *Ifitm2* with the canonical Wnt signaling pathway contributing to osteogenic differentiation. However, how IFITM2

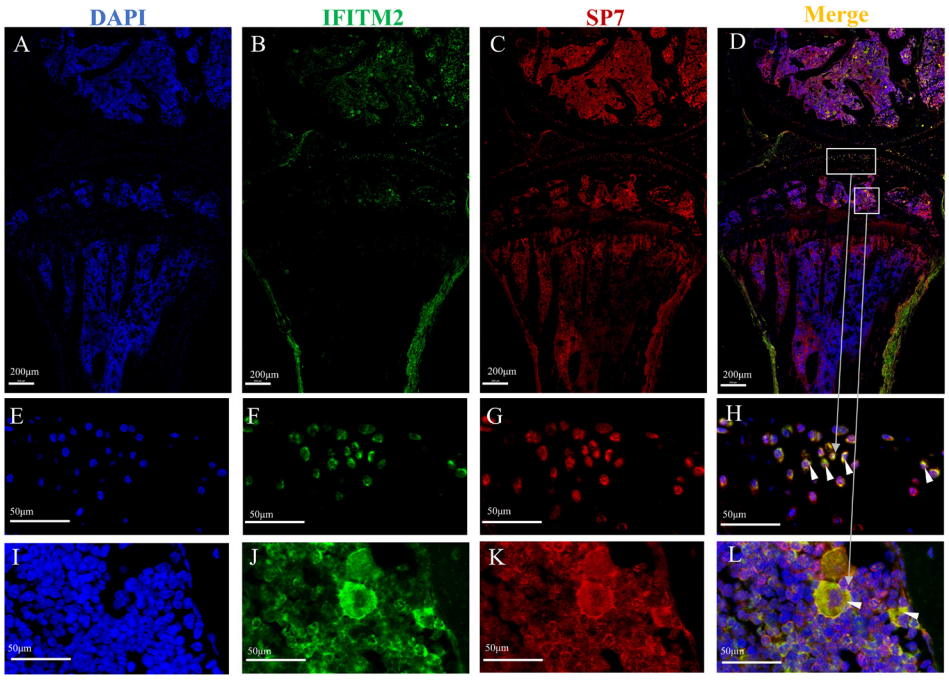


**Figure 5. Expression of IFITM2 examined by histology in mice. (A–D)** Representative immunofluorescence staining of IFITM2 (green) and SP7 (red) in the hind limb bone of 15-week-old mice. Scale bars, 200 μm. **(E–H)** Articular cartilage and **(I–L)** metaphyseal bone regions magnified to display positive cells. White arrow indicates IFITM2 and SP7 co-localization in endochondral ossification centers and articular cartilage. Scale bar: 50 μm. DAPI (blue) was used to counterstain nuclei.

interacts with the Wnt signaling pathway and whether it has similar mechanisms to IFITM5 in osteogenic differentiation remain unclear.

IFITM protein overexpression promotes interferon-β production (*37*). In early osteoblastic differentiation, IFN inhibits ECM synthesis, leading to delayed bone formation (*38*). Hence, we hypothesized that upregulated expression of IFITM2 during osteogenic differentiation may be independent of interferon and involve the canonical Wnt signaling pathway. A shortcoming of this study is that further experiments are needed to support an association between the canonical Wnt signaling pathway and overexpression or knockdown of *Ifitm2*, and we did not reveal the relationship between *Ifitm2* and Wnt the signaling pathway in detail.

*Funding*: This work was supported by a grant from the Natural Science Foundation of Shandong Province (General program ZR2023MH276) and Academic Promotion Program of Shandong First Medical University (LJ001).

*Conflict of Interest*: The authors have no conflicts of interest to disclose.

**References**

1. Pittenger MF, Mackay AM, Beck SC, Jaiswal RK, Douglas R, Mosca JD, Moorman MA, Simonetti DW, Craig S, Marshak DR. Multilineage potential of adult human mesenchymal stem cells. Science. 1999; 284:143-147.
2. Amarasekara DS, Kim S, Rho J. Regulation of Osteoblast Differentiation by Cytokine Networks. Int J Mol Sci. 2021; 22.
3. Huang W, Yang S, Shao J, Li YP. Signaling and transcriptional regulation in osteoblast commitment and differentiation. Front Biosci. 2007; 12:3068-3092.
4. Stein GS, Lian JB. Molecular mechanisms mediating proliferation/differentiation interrelationships during progressive development of the osteoblast phenotype. Endocr Rev. 1993; 14:424-442.
5. Rutkovskiy A, Stensløkken KO, Vaage IJ. Osteoblast Differentiation at a Glance. Med Sci Monit Basic Res. 2016; 22:95-106.
6. Glass DA, 2nd, Bialek P, Ahn JD, Starbuck M, Patel MS, Clevers H, Taketo MM, Long F, McMahon AP, Lang RA, Karsenty G. Canonical Wnt signaling in differentiated osteoblasts controls osteoclast differentiation. Dev Cell. 2005; 8:751-764.
7. Lin X, Patil S, Gao YG, Qian A. The Bone Extracellular Matrix in Bone Formation and Regeneration. Front Pharmacol. 2020; 11:757.
8. Takayanagi H, Kim S, Matsuo K, Suzuki H, Suzuki T, Sato K, Yokochi T, Oda H, Nakamura K, Ida N, Wagner EF, Taniguchi T. RANKL maintains bone homeostasis through c-Fos-dependent induction of interferon-beta. Nature. 2002; 416:744-749.
9. Kota SK, Roening C, Patel N, Kota SB, Baron R. PRMT5 inhibition promotes osteogenic differentiation of mesenchymal stromal cells and represses basal interferon stimulated gene expression. Bone. 2018; 117:37-46.
10. Deng Z, Ng C, Inoue K, Chen Z, Xia Y, Hu X, Greenblatt M, Pernis A, Zhao B. Def6 regulates endogenous type-I interferon responses in osteoblasts and suppresses osteogenesis. eLife. 2020; 9.
11. Zhao X, Li J, Winkler CA, An P, Guo JT. IFITM Genes, Variants, and Their Roles in the Control and Pathogenesis of Viral Infections. Front Microbiol. 2018; 9:3228.
12. Liao Y, Goraya MU, Yuan X, Zhang B, Chiu SH, Chen JL. Functional Involvement of Interferon-Inducible Transmembrane Proteins in Antiviral Immunity. Front Microbiol. 2019; 10:1097.
13. Bailey CC, Zhong G, Huang IC, Farzan M. IFITM-Family Proteins: The Cell's First Line of Antiviral Defense. Annu Rev Virol. 2014; 1:261-283.
14. Lu Y, Zuo Q, Zhang Y, Wang Y, Li T, Han J. The expression profile of IFITM family gene in rats. Intractable Rare Dis Res. 2017; 6:274-280.
15. Warren CJ, Griffin LM, Little AS, Huang IC, Farzan M, Pyeon D. The antiviral restriction factors IFITM1, 2 and 3 do not inhibit infection of human papillomavirus, cytomegalovirus and adenovirus. PloS One. 2014; 9:e96579.
16. Prelli Bozzo C, Nchioua R, Volcic M, *et al*. IFITM proteins promote SARS-CoV-2 infection and are targets for virus inhibition *in vitro*. Nat Commun. 2021; 12:4584.
17. Gómez-Herranz M, Taylor J, Sloan RD. IFITM proteins: Understanding their diverse roles in viral infection, cancer, and immunity. J Biol Chem. 2023; 299:102741.
18. Zhang Y, Lu Y, Li X, Zhang S, Liu P, Hao X, Han J. The novel role of IFITM1-3 in myogenic differentiation of C2C12 cells. Intractable Rare Dis Res. 2023; 12:180-190.
19. Kim D, Paggi JM, Park C, Bennett C, Salzberg SL. Graph-based genome alignment and genotyping with HISAT2 and HISAT-genotype. Nat Biotechnol. 2019; 37:907-915.
20. Liao Y, Smyth GK, Shi W. featureCounts: An efficient general purpose program for assigning sequence reads to genomic features. Bioinformatics (Oxford, England). 2014; 30:923-930.
21. Robinson MD, McCarthy DJ, Smyth GK. edgeR: a Bioconductor package for differential expression analysis of digital gene expression data. Bioinformatics (Oxford, England). 2010; 26:139-140.
22. Ding DC, Shyu WC, Lin SZ. Mesenchymal stem cells. Cell Transplant. 2011; 20:5-14.
23. Chmielewska AM, Gómez-Herranz M, Gach P, Nekulova M, Bagnucka MA, Lipińska AD, Rychłowski M, Hoffmann W, Król E, Vojtesek B, Sloan RD, Bieńkowska-Szewczyk K, Hupp T, Ball K. The Role of IFITM Proteins in Tick-Borne Encephalitis Virus Infection. J Virol. 2022; 96:e0113021.
24. Smith SE, Busse DC, Binter S, *et al*. Interferon-Induced Transmembrane Protein 1 Restricts Replication of Viruses That Enter Cells *via* the Plasma Membrane. J Virol. 2019; 93.
25. Tartour K, Cimarelli A. IFITM, a common barrier to many viruses. Med Sci (Paris). 2015; 31:377-382. (in French)
26. Moffatt P, Salois P, Gaumond MH, St-Amant N, Godin E, Lanctôt C. Engineered viruses to select genes encoding secreted and membrane-bound proteins in mammalian cells. Nucleic Acids Res. 2002; 30:4285-4294.
27. Hanagata N, Takemura T, Monkawa A, Ikoma T, Tanaka J. Phenotype and gene expression pattern of osteoblast-like cells cultured on polystyrene and hydroxyapatite with pre-

adsorbed type-I collagen. J Biomed Mater Res A. 2007; 83:362-371.
28. Kim EJ, Lee MJ, Kim HY, Green DW, Takata T, Jung HS. Inhibitory effect of IFITM5 on cementoblast differentiation is associated with Wnt signaling. Acta Biochim Biophys Sin (Shanghai). 2018; 50:1176-1179.
29. Zhou Y, Lin J, Shao J, Zuo Q, Wang S, Wolff A, Nguyen DT, Rintoul L, Du Z, Gu Y, Peng YY, Ramshaw JAM, Long X, Xiao Y. Aberrant activation of Wnt signaling pathway altered osteocyte mineralization. Bone. 2019; 127:324-333.
30. Zhang R, Yang G, Wu X, Xie J, Yang X, Li T. Disruption of Wnt/β-catenin signaling in odontoblasts and cementoblasts arrests tooth root development in postnatal mouse teeth. Int J Biol Sci. 2013; 9:228-236.
31. Koo BK, Spit M, Jordens I, Low TY, Stange DE, van de Wetering M, van Es JH, Mohammed S, Heck AJ, Maurice MM, Clevers H. Tumour suppressor RNF43 is a stem-cell E3 ligase that induces endocytosis of Wnt receptors. Nature. 2012; 488:665-669.
32. Schelle L, Abrantes J, Baldauf HM, Esteves PJ. Evolution of primate interferon-induced transmembrane proteins (IFITMs): A story of gain and loss with a differentiation into a canonical cluster and IFITM retrogenes. Front Microbiol. 2023; 14:1213685.
33. Siegrist F, Ebeling M, Certa U. The small interferon-induced transmembrane genes and proteins. J Interferon Cytokine Res. 2011; 31:183-197.
34. Liang T, Wang X, Wang Y, Ma W. IFN-γ Triggered IFITM2 Expression to Induce Malignant Phenotype in Elderly GBM. J Mol Neurosci. 2023; doi: 10.1007/s12031-023-02156-5.
35. Daniel-Carmi V, Makovitzki-Avraham E, Reuven EM, Goldstein I, Zilkha N, Rotter V, Tzehoval E, Eisenbach L. The human 1-8D gene (IFITM2) is a novel p53 independent pro-apoptotic gene. Int J Cancer. 2009; 125:2810-2819.
36. Liu Y, Zhou M, Wu J, Wen Z, Fang Y, Lin L, Luo M, Sun L, Liao W. Interferon-induced transmembrane protein 2 promotes epithelial-mesenchymal transition by activating transforming growth factor-β1/small mother against decapentaplegic 2 signaling in gastric cancer. Mol Biol Rep. 2022; 49:997-1006.
37. Chen L, Li X, Deng Y, Bi Y, Yan Z, Yang Y, Zhang X, Li H, Xie J, Feng R. IFITM2 Presents Antiviral Response through Enhancing Type I IFN Signaling Pathway. Viruses. 2023; 15:866.
38. Woeckel VJ, Eijken M, van de Peppel J, Chiba H, van der Eerden BC, van Leeuwen JP. IFNβ impairs extracellular matrix formation leading to inhibition of mineralization by effects in the early stage of human osteoblast differentiation. J Cell Physiol. 2012; 227:2668-2676.

Received November 22, 2023; Revised December 20, 2023; Accepted December 22, 2023.

*Address correspondence to:
Yanqin Lu and Jinxiang Han, The First Affiliated Hospital of Shandong First Medical University & Shandong Provincial Qianfoshan Hospital, No. 16766 Jingshi Road, Ji'nan, Shandong 250013, China.
E-mail: yqlu@sdfmu.edu.cn (LYQ), jxhan@sdfmu.edu.cn (HJX)

Released online in J-STAGE as advance publication December 25, 2023.